Review on the materials composition and performance evolution of green alkali-activated cementitious materials

Xiaoniu Yu[1], Jinyan Shi[2*], Zhihai He[3*], Çağlar Yalçınkaya[4], Víctor Revilla-Cuesta[5], Osman Gencel[6]

[1]Jiangsu Key Laboratory of Construction Materials, Nanjing 211189, China

[2]School of Civil Engineering, Central South University, Changsha 410075, China

[3]College of Civil Engineering, Shaoxing University, Shaoxing 312000, China

[4]Department of Civil Engineering, Dokuz Eylül University, Izmir, Turkey

[5]Department of Civil Engineering, Escuela Politécnica Superior, University of Burgos, c/ Villadiego s/n, 09001 Burgos, Spain

[6]Bartin University, Department of Civil Engineering, Bartin 74100, Turkey

Abstract: Alkali-activated cementitious materials (AAMs) are a kind of low-carbon building materials. This review considers the related research on the AAMs to systematically summarize the results on its materials composition and performance influencing factors. The precursor material is mainly industrial solid waste containing Al_2O_3 and SiO_2. The alkali activator (AA) is compounds containing caustic alkali and basic elements, which can provide alkaline environment. Meanwhile, some new green precursors and AAs are summarized in this review. The main mechanism of alkali-activated reaction is that the hydroxide ion from the AA nucleophilically attacks the covalent bonds of Al-O and Si-O in the precursor material, which generates $Si(OH)_4$ and $Al(OH)_4^-$. They generate three-dimensional network gel of tetrahedral structure of $[SiO_4]$ and $[AlO_4]^-$ through polycondensation reaction, which form cement stone-like block material after setting and hardening. Too high or too low AA concentration is detrimental to the workability and mechanical properties of AAMs. When the ratio of Na/K to Al is small, the mechanical properties of AAMs is reduced. When the Ca content in the AAM is high, calcium ions enter the polycondensation chain and reduce the degree of polymerization and mechanical properties of the aluminosilicate gel phase and increase the shrinkage deformation. The hydration products in the AAM are free of calcium hydroxide, calcium aluminate hydrate, ettringite, etc., and can resist the erosion of acid and sulfate media. With the development of the theory and technology of AAMs, it may be used to completely replace ordinary Portland cement in the future.

*Corresponding author.
E-mail address: jinyan.shi@csu.edu.cn (Jinyan Shi).

1. Introduction

Ordinary Portland cement (OPC) is the most widely used construction cementing material in the world and can be used in the construction of dam, airport, and other engineering fields (Wang et al., 2020). The coal is burned to calcinate limestone during the production process of OPC. In the process, a large amount of carbon dioxide is released. Meanwhile, a large amount of solid waste, such as fly ash (FA), is also generated. In the cement industry, around 800 kg of carbon dioxide is produced for every production 1000 kg of OPC, which accounts for around 6%−9% of global carbon dioxide (Geng et al., 2019). The carbon dioxide is a greenhouse gas, which can increase the earth temperature, cause frequent natural disasters, and pose a serious threat to people lives and properties. Therefore, low-carbon, zero-carbon or negative-carbon building cementitious materials are needed to replace OPC completely or partially according to the properties of different engineering fields. Precursor materials are mainly based on industrial solid wastes containing silica and aluminum oxide as raw materials (Deng et al., 2021; Gavali et al., 2021). These materials are not gelatinous or have very weak cementing properties. When alkaline compounds are used as activators, precursor materials are stimulated to form the same or similar chemical composition of the hydration product of OPC (Calcium silicate hydrate (C-S-H) gel), which is named as AAMs (Parathi et al., 2021). Therefore, they are low-carbon building cementitious materials.

In the 1940s, alkaline materials are firstly mixed with slag and then the AAM is prepared (Zhang et al., 2020). In the 1950s, the industrial production of AAMs is realized by the former Soviet Union for the first time (Zhang et al., 2020). At the end of the 1970s, the aluminosilicate material is used as the precursor, which has $[SiO_4]^{4-}$ and $[AlO_4]^{5-}$ structures. Under the action of the alkali activator (AA), a new type of three-dimensional network structure of the polyaluminosilicate cementitious material is prepared. Therefore, hydration products structure of some AAMs is significantly different from OPC, so they have specific properties, such as high strength, low heat of hydration, and good durability. Its preparation process is simple, and emissions of CO_2 can be reduced during the production process compared to OPC, which is one of the important ways to achieve carbon emission reduction (Xue et al., 2021). Meanwhile, the resource utilization of solid

59   wastes can be realized. In recent years, the research and application of AAMs have attracted

60   extensive attention from civil engineers.

61   Recently, the research on AAM is very active, and it is constantly developing towards low-

62   carbon, eco-friendly, and high-performance. Shi et al. (2019a) systematically reviewed low-carbon

63   cementitious components and proved that AAM plays an important role in the sustainable

64   development of building materials. Albidah (2021) reviewed the impact of alternative materials on

65   the freshness and mechanical properties of AAMs. Meanwhile, because AAM paste tends to have

66   high viscosity and hardening rate, Lu et al. (2021) reviewed the ways to improve the rheological

67   properties of AAM. Li et al. (2019a) focused on summarizing the mixture design method of alkali-

68   activated FA- round-granulated blast furnace slag (GGBS) binder, and considered the properties of

69   raw materials, the type and amount of activator, and the curing regime. In addition, Fu et al. (2021)

70   reviewed the microstructure evolution and durability of FA-based geopolymer. Further, Zhang et al.

71   (2017) and Tahri et al. (2021) reviewed the long-term service performance of AAM in complex

72   environments, and discussed the corrosion of steel bars, alkali-silicon reaction, permeability and

73   resistance to carbonization. As the research of AAM is updated rapidly, it is necessary to review the

74   latest material composition and performance influencing factors on AAMs.

75   The domestic and foreign research progress on the selection of raw materials and performance

76   influencing factors of AAMs is reviewed. Looking forward to the future development prospects of

77   AAMs. In terms of the selection of raw materials, the commonly used raw materials for AAMs

78   include FA, metakaolin (MK), GGBS, and other industrial wastes containing high silicon/aluminum

79   and low calcium. Commonly used AAs are sodium hydroxide, calcium hydroxide, sodium carbonate,

80   water glass, and their mixtures. Meanwhile, some new green precursors and AAs are summarized.

81   In terms of performance influencing factors, the type and concentration of the AA, the ratio of

82   Si/Na/K to Al, the content of Ca, and the type and content of water have a greater impact on AAMs.

83   Therefore, AAMs can be used to replace OPC, which is a type of low-carbon cementitious materials

84   that meets green and sustainable development.

85

86   **2. Selection of raw materials**

87   Two key components of AAMs: (a) precursor materials (aluminosilicate source), solid waste

88   that may contain Al, Si, and Ca, et al.; (b) AA (alkaline solutions), e.g. NaOH, KOH, Na_2SiO_3,

89   K_2SiO_3, et al. In addition, like traditional cement-based materials (CBMs), aggregates such as sand

90   and crushed stone are also necessary for AAMs.

91   *2.1. Precursor materials*

92   Ternary diagram of SiO_2-Al_2O_3 and Fe_2O_3-CaO containing in precursor materials is presented

93   in Fig. 1. The commonly used precursor materials are aluminosilicate materials contained FA, MK,

94   GGBS, rice husk ash (RHA), and palm oil fuel ash (POFA).
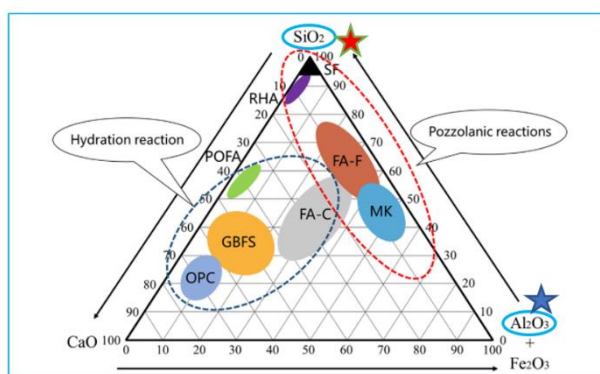
95

96   Fig. 1. Ternary diagram of SiO_2-Al_2O_3 and Fe_2O_3-CaO containing in precursor materials.

97   *2.1.1. Fly Ash*

98   The FA is formed by pulverized coal entering the furnace at 1300–1500 ℃, after being

99   subjected to heat absorption by the hot surface under suspension combustion conditions, and it is

100   then cooled. The 250–300 kg of the FA usually needs to burn 1 ton of coal. It mainly comes from

101   the tiny ash particles collected in the flue gas of coal-fired power plants. The main chemical

102   components of FA are oxides of silicon, aluminum, iron, calcium, magnesium, etc., as shown in Fig.

103   2(b) (Temuujin et al., 2004). It has potential chemical activity. The morphology is mainly in the

104   form of spherical structure with diameter in the range of 1–20 μm (Fig. 2(a)), which is generally

105   beneficial to the fluidity of AAMs (Temuujin et al., 2004). The FA can be divided into low-

106   calcium/high-calcium FA according to the content of CaO or free CaO. For example, the content of

107   CaO (>8%) or content of free CaO (>1%) is the high calcium FA. Generally, the low-calcium FA

108   is used as the precursor material when the FA-based AAM is prepared, as listed in Table S1

109   (Supplementary File). However, due to the fast setting speed and high availability of class C high

110   calcium-FA under alkaline conditions, it has not been widely used as the precursor materials

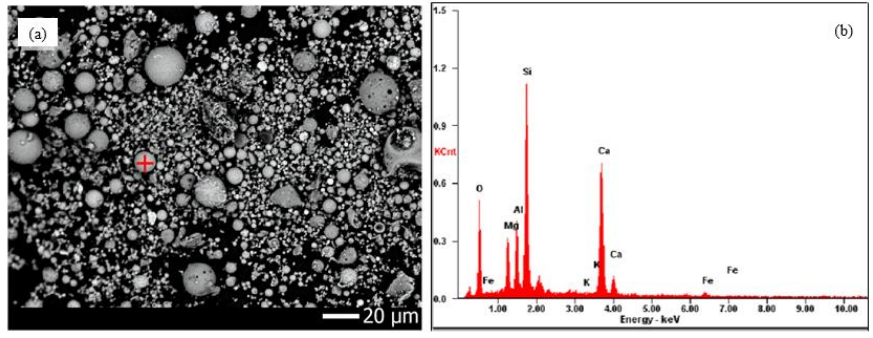111   (Rattanasak et al., 2011).

Fig. 2. SEM and EDS image of FA (Temuujin et al., 2004).

2.1.2. Metakaolin

The MK is anhydrous aluminum silicate ($Al_2O_3 \cdot 2SiO_2$) formed by dehydrating kaolin ($Al_2O_3 \cdot 2SiO_2 \cdot 2H_2O$) at 800 °C for 6 h. The molecular arrangement of the MK is irregular (Fig. 3(a)), it presents a thermodynamic metastable state, and has cementing properties in the AAM (Wianglor et al., 2017). Due to the amorphous phase hump in the XRD pattern (Fig. 3(b)), MK has higher reactivity under alkaline conditions (Gbozee et al., 2018). The network structure of the aluminosilicate gel can be formed by depolymerization-polymerization process when the metastable state of the MK is reacted with AAs. The metakaolin in the concrete is a powdered state and usually has the small size and high specific surface area.
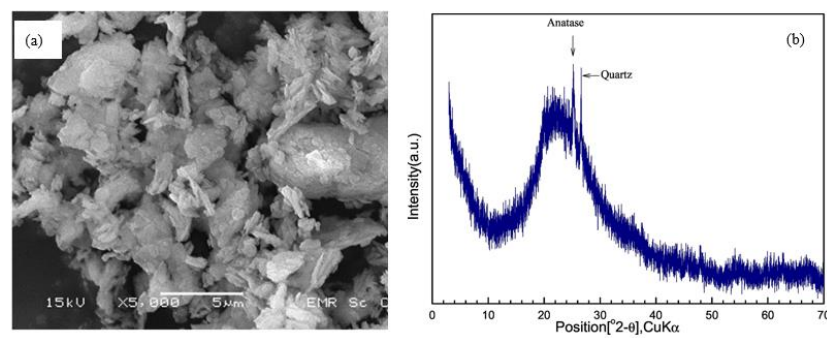

Fig. 3. SEM and XRD image of MK (Wianglor et al., 2017; Gbozee et al., 2018).

2.1.3. Ground-granulated blast furnace slag

The GGBS is the micronized slag powder with a high-fineness and high-activity obtained by water-quenched blast furnace slag. The GGBS is a traditional industrial waste residue, which is a pozzolanic active material. GGBS is the angular and irregular particle with a smooth surface, as presented in Fig. 4(a) (Deng et al., 2021). It contains active SiO_2 and Al_2O_3 (Fig. 4(b)), which can chemically react with the AA at room or high temperature to form gels with a stable structure. For

132 example, the GGBS can be activated by lime containing high amount of CaO, and the C-S-H gel is

133 then produced (Kogbara and Al-Tabbaa, 2011). Therefore, the GGBS can be used as a precursor

134 material.
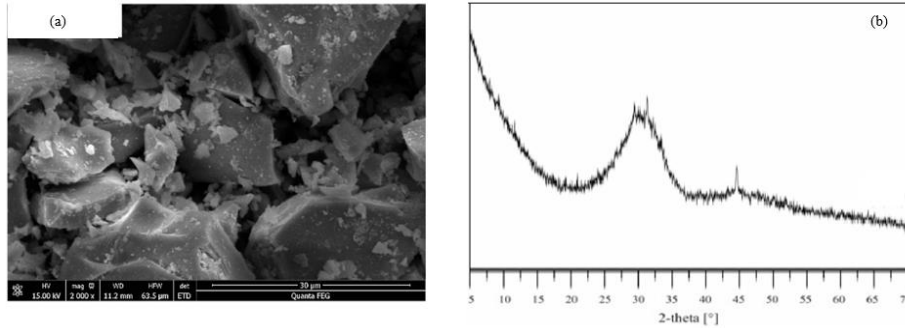
136 Fig. 4. SEM and XRD image of GGBS (Deng et al., 2021).

137 *2.1.4. Biomass ash*

138 Globally, agriculture produces approximately 140 billion metric tons of biomass waste each

139 year, and the ash produced by calcination of these agricultural wastes is called biomass ash

140 (Martirena and Monzó, 2018). Rice is the main food crop in Asia, and the ash from the burning of

141 its shell is called RHA. According to the different calcination temperature, as the internal carbon

142 content decreases, its color gradually changes from black to white. Meanwhile, during the

143 calcination process, the decomposition of organic matter leaves a large number of small pores inside

144 the RHA, as presented in Fig. 5 (Kang et al., 2019; Lertwattanaruk et al., 2018). Therefore, RHA

145 has a higher porosity and specific surface area, so that it has a water retention function and plays an

146 internal curing role in the cementitious component. The reactivity of RHA is closely related to its

147 amorphous SiO_2 content, which is affected by the calcination temperature (Table 1) (Martirena and

148 Monzó. 2018). Generally, RHA obtained with a calcination temperature of 600–700 °C has good

149 pozzolanic activity. Higher calcination temperature (800–1000 °C) leads to the crystallization of

150 SiO_2 similar to cristobalite and phosphate quartz in RHA, thereby reducing reactivity. In addition,

151 RHA generally contains a small amount of KOH, which is also beneficial to increase the pH value

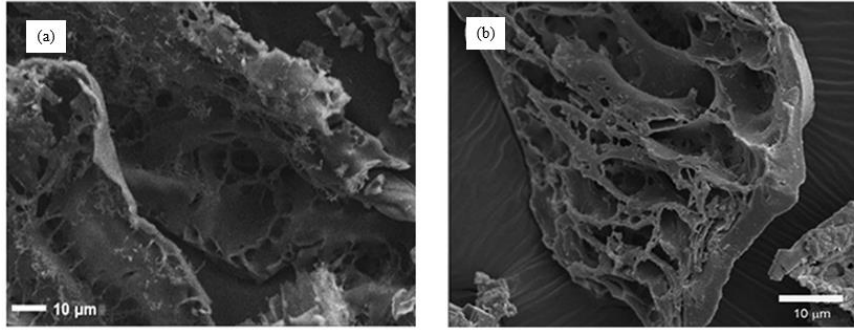152 of the system and make RHA react further.

Fig. 5. SEM and XRD image of RHA (Lertwattanaruk et al., 2018; Kang et al., 2019).

Table 1. The influence of calcination temperature on the chemical composition and activity index of RHA.

Calcination temperature (Time)	Al$_2$O$_3$	SiO$_2$	CaO	Fe$_2$O$_3$	K$_2$O	MgO	P$_2$O$_5$	SO$_3$	Na$_2$O	LOI	28-d NCS	Ref.
500 ℃ (120 min)	—	89.47	2.69	0.62	0.83	1.16		0.93	2.09	2.27	1.26 (10%)	Muthadhi and Kothandaraman. (2010)
600 ℃ (60 min)	0.1	92.09	0.97	0.07	4.04	0.53	0.96	0.55	0.11	1.52	1.1 (10%)	Bie et al. (2015)
600 ℃ (120 min)	0.1	93	0.92	0.07	3.62	0.45	0.91	0.46	—	1.48	1.23 (10%)	Bie et al. (2015)
700 ℃ (60 min)	0.12	93.42	0.92	0.07	3.26	0.37	0.68	0.44	0.27	3.24	1.07 (5%)	Bie et al. (2015)
800 ℃ (40 min)	0.26	92.4	1.63	0.3		0.38		0.11	1.24		1.35 (15%)	Venkatanarayanan and Rangaraju. 2015

* NCS: 28-d normalized compressive strength (replacement level).

POFA is also a common biomass ash used in AAMs. The morphology of POFA is spherical, and its main crystalline phases are cristobalite and quartz, while some researchers think that they are mullite and quartz (Fig. 6) (Sarde et al., 2021).
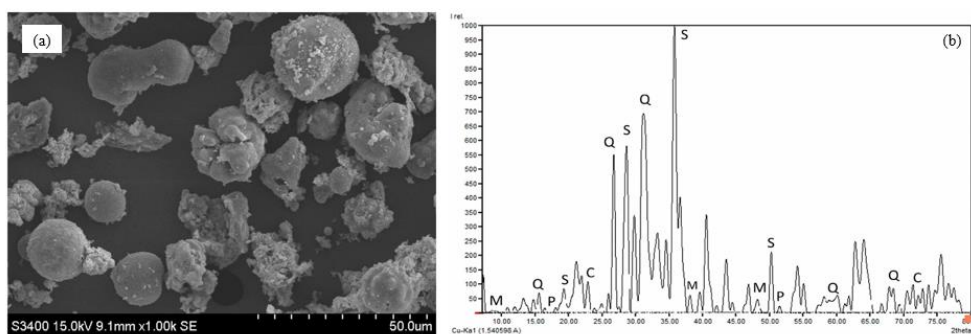

Fig. 6. SEM and XRD image of POFA (Sarde et al., 2021).

162   Sugarcane is the largest crop in the world, and the ash that is burned after extracting syrup from

163   bagasse is called sugarcane bagasse ash (SCBA). Meanwhile, the ashes produced by burning end-

164   cuts of canes and sugarcane leaves are called sugarcane straw ash (SCSA) (Cordeiro et al., 2017).

165   Both SCBA and SCSA are porous structures and contain a large amount of amorphous SiO_2, which

166   makes them have the potential as a precursor. Due to the difference in calcination temperature,

167   SCBA may contain different contents of crystal phases (e.g. quartz and cristobalite). Villar-Cocina

168   et al. (2008) believed that when the calcination temperature was 800–1000 °C, the performance of

169   SCBA was better. Meanwhile, the SiO_2 content in SCSA and SCBA is low, which can improve its

170   purity by pretreatment. The researchers found that the content of SiO_2 without pretreatment was

171   73.4%, while the SiO_2 content after hot water washing and acid treatment was 83% and 95%,

172   respectively (Cordeiro et al., 2017).

173   The use of biomass ash to replace the main precursor has become a trend, because in most

174   countries, biomass power plants produce a large amount of biomass ash every year. Meanwhile,

175   crop wastes such as olives, corn ears, corn stalks and cotton husks all produce ash after being burned,

176   and contain part of active SiO_2, but they contain high potassium content, which makes it possible to

177   replace activators.

178   *2.1.5. Other solid waste powder*

179   A large amount of solid waste powder with SiO_2 and Al_2O_3 as the main components is used to

180   produce AAMs, such as waste glass powder (WGP), water treatment sludge powder (WTS) and so

181   on (Abbas et al., 2020). The city produces a large amount of solid waste every day, which becomes

182   municipal solid waste incineration fly ash (MSWI) after being processed and incinerated (Jiang et

183   al., 2019). The researchers used MSWI to replace the main precursor to prepare AAMs, and verified

184   the feasibility of using MSWI to prepare AAMs, as listed in Table S2 (Supplementary File).

185   Pretreatment methods such as washing can reduce the chloride and sulfide content in MSWI, thereby

186   improving its reactivity under alkaline conditions (Jiang et al., 2019).

187   With the development of urbanization and industry, a variety of sludge solid wastes are adopted

188   as precursors in AAMs, for example, WTS (Pham et al., 2021), dredged sludge (Lang et al., 2021),

189   and papermaking sludge. Mañosa et al. (2021) used WTS to replace part of clay to prepare AAMs,

190   and found that Al_2O_3 and CaO in WTS promoted the formation of C-A-S-H and C-S-H gels.

191   Meanwhile, the reaction activity of WTS can also be increased through acid treatment and heat

treatment, so that it can exert pozzolanic activity. The main components of many kinds of sludge are SiO_2 and Al_2O_3, but due to differences in the raw materials and treatment processes, they also contain CaO and Fe_2O_3 (as presented in Table 2). The content of SiO_2 and Al_2O_3 in WTS is relatively high, while the content of CaO in dredged sludge, waste sandstone sludge, and paper sludge ash is relatively high, and part of the sludge contains heavy metal ions.

Table 2. The main chemical components of municipal sludge.

Sludge	SiO_2	Al_2O_3	CaO	K_2O	Fe_2O_3	SO_3	CuO	MgO	Na_2O	TiO_2	PbO	CeO_2	MnO	La_2O_3	P_2O_5	LOI	Ref.
DS	42.2	21.6	7.2	8.2	12.8			2	3							3.1	Lang et al. (2021)
UWTS	26.4	28.3	5.4	1.2	7.7	0.5	0.71	1.1								29.5	Pham et al. (2021)
CWTS	31.1	47.7	4.3	1	5	3.4	0.3	1								6.2	Pham et al. (2021)
CWTS	59	24.6	0.7	1.5	6.6			1.1	4.1	1.4						1.4	Nimwinya et al. (2016)
GS	41.2	1.2	3.7	3.9	8.6	0.4		0.3	1.1	18.7		4.7	0.3	1.8		14	Saleh et al. (2021)
WSS	43.5	8.3	19.5	1.7	2.4	0.2		4.2		0.4						18	Clausi et al. (2018)
PSA	16.4-25.7	9.1-18.9	43.5-61.2	0.2-1.3	0.4-0.9	0.2-1.1		2.7-5.2	0.1-1.6	0.3-0.7			0.04		0.1-0.5	0.01-1.03	Mengasini et al. (2021)

* DS: Dredged sludge, UWTS: Untreated WTS, CWTS: Calcined WTS, GS: Glass sludge, WSS: Waste sandstone sludge, PSA: Paper sludge ash.

At present, WGP from a variety of sources is used to produce low-carbon AAMs, including windows glass, container glass, display screens, cathode tubes, and fluorescent lamp glass, etc (Sun et al., 2017). Because WGP is rich in SiO_2 and alkali metal oxide (e.g. Na_2O), gel nucleation occurs around it. Tho-In et al. (2018) used container glass and fluorescent lamp glass to replace part high-calcium FA to prepare low-carbon AAM, and found that the performance of specimens prepared with 20% of container glass was better than that of the control and experimental groups with

206 fluorescent lamp glass. Sun et al. (2017) found that under the condition of alkali activation, the

207 surface of glass particles was accumulated by continuous size gel particles to form a relatively

208 smooth gel surface. Under the same conditions, the surface of the WGP was relatively rough,

209 consisting of 2–3 μm spherical gel particles (as presented in Fig. 7). This was mainly due to the

210 rapid dissolution of SiO_2 in the glass under alkaline conditions, which caused the product to

211 precipitate on its surface.
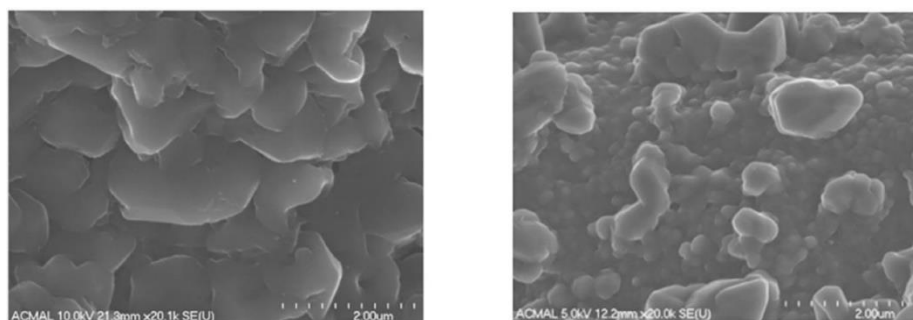
212

213 Fig. 7. SEM image of glass particle (a), and glass powder (b) (Sun et al., 2017).

214 At present, highly active GGBS and FA are still the main precursors in AAMs, while other

215 materials with high-content Al_2O_3 and SiO_2 are used as partial substitutes. Two or more precursor

216 materials can be mixed to meet the corresponding engineering requirements after being ground into

217 powder by adjusting the Al/Si ratio in SiO_2 and Al_2O_3.

218 *2.2. Alkali activator*

219 The AA is similar with chemical catalysts, usually is caustic alkali and basic elements such as

220 sodium silicate, sodium hydroxide, and so on. The AA activates the precursor material to form a

221 cementitious material. It has an important influence on the type, mechanical properties, thermal

222 properties, volume stability, setting time, etc. of AAMs. The hydroxide ions in the AA can

223 nucleophilically attack covalent bonds of Al_2O_3 and SiO_2 in the precursor material, causing them to

224 break. The binary/ternary-based AAs are often used to activate precursor materials.

225 *2.2.1. Hydroxide activators*

226 The dissolution of hydroxide activators (e.g., NaOH, CaOH, KOH, LiOH, CsOH, RbOH)

227 produces OH$^-$ to promote the dissolution of the precursor, which is caused by the mutual diffusion

228 and ion exchange of solutes (such as alkali cations, H_2O and OH$^-$) and aluminosilicate network

229 modifier cations (such as Ca^{2+} or Na^+), as shown in Eq. (1). In an alkaline environment, the Si and

230 O bonds in the aluminosilicate are broken, as presented in Fig. 8 (Garcia-Lodeiro et al., 2015).

231   Meanwhile, -O-Si and -OH attract electrons to make Si atoms lose electrons. When the dissolved

232   monomer or alumina ($Al(OH)^{4-}$) and oligomeric silicate reach a certain concentration, they

233   combines to form a new aluminosilicate network (intermediate structures, C-A-S-H, or N-A-S-H)

234   and release some hydroxyl groups (Garcia-Lodeiro et al., 2015).

235    $$Na^+ \text{ (aluminosilicate network)} + H_2O \text{ (aq)} \rightleftharpoons H^+ \text{ (aluminosilicate network)} + NaOH \text{ (aq)} \quad (1)$$
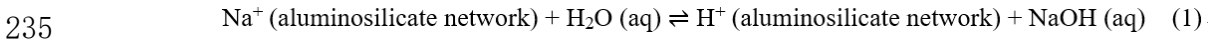
236   Generally speaking, as the alkalinity of the activator increases, the dissolution of the precursor

237   increases. However, researchers think that the concentration of alkali hydroxide should match the

238   concentration of soluble Al in the system, so that the molar ratio of Al/alkali metal in the binder is

239   about 1. In addition, high alkalinity may cause flowering in AAMs, and also reduce the degree of

240   polymerization of silicate (substrate spacing of C-(N)-(A)-S-H gel and average silicate chain length),

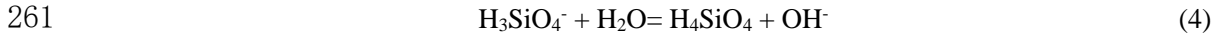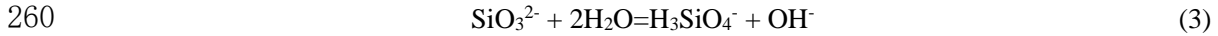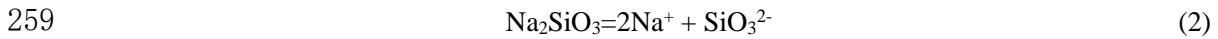241   which is detrimental to the long-term durability of AAMs.
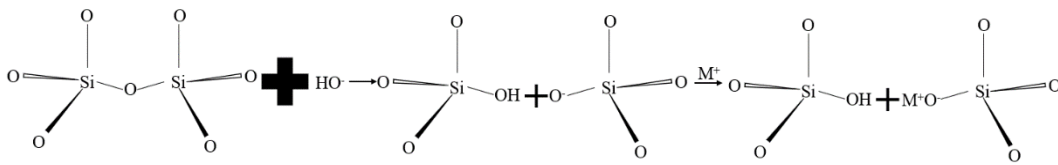
243   Fig. 8. The schematic diagram of the Si–O–Si bond breakage by the action of OH^-.

244   *2.2.2. Silicate activators*

245   Sodium silicate ($Na_2O \cdot xSiO_2$) is one of the most commonly used silicate activators, and its

246   aqueous solution is usually called water glass. It can ionize hydroxide ions in water, which can break

247   the covalent bonds of Al_2O_3 and SiO_2 in the precursor material (Eqs. 2–4). The modulus x in the

248   sodium silicate is the molar ratio of SiO_2 to Na_2O, indicating its composition ratio. The larger the

249   modulus, the more difficult to dissolve in water. When the x is 1, the sodium silicate can dissolve

250   at room temperature. At x>3, steam above 4 atmospheres are needed to dissolve. Meanwhile, the

251   greater modulus of sodium silicate, the greater content of silicon content, and its viscosity is high.

252   Therefore, the sodium silicate corresponding modulus is selected as the AA according to the

253   properties of the precursor material. For example, an industrial-grade sodium silicate solution is

254   used as an AA, and its modulus is 2.2 (Yan et al., 2021). Concentration and molar ratio (SiO_2/M_2O,

255   M is Na or K) are important indicators to control the effect of silicate activators, and the two

256   indicators affect each other. i.e., when silica modulus does not change, an increase in concentration

257 increases the viscosity of the activator and make it unstable. Usually, alkali hydroxide is used to

258 adjust the modulus of silicate activators, thereby depolymerizing the polysilicate species.

$$Na_2SiO_3=2Na^+ + SiO_3^{2-} \tag{2}$$

$$SiO_3^{2-} + 2H_2O=H_3SiO_4^- + OH^- \tag{3}$$

$$H_3SiO_4^- + H_2O= H_4SiO_4 + OH^- \tag{4}$$

262 *2.2.3. Carbonate activators*

263   Only a few carbonates such as Na_2CO_3 and K_2CO_3 can be fully dissolved in water, however, a

264 few slightly soluble carbonates (Li_2CO_3) are also used as activators. The Na_2CO_3 is known as soda

265 ash, is easily soluble and ionize in water. Finally, carbonate and hydroxide ions are produced, so the

266 pH of the solution is alkaline, as shown in Eqs. (5–7). The hydroxide ions in sodium carbonate can

267 nucleophilically attack to destroy the covalent bonds of Al_2O_3 and SiO_2. The strength development

268 and setting time of AAMs can be delayed when Na_2CO_3 is selected as an AA, which has attracted

269 less attention (Akturk et al., 2020). However, since the carbonate solution is relatively low in

270 alkalinity, its activation effect on the low-calcium precursor is relatively low.

$$Na_2CO_3=2Na^+ + CO_3^{2-} \tag{5}$$

$$CO_3^{2-} + H_2O=HCO_3^- + OH^- \tag{6}$$

$$HCO_3^- + H_2O= H_2CO_3 + OH^- \tag{7}$$
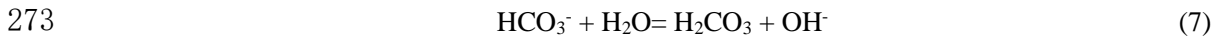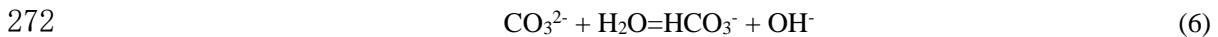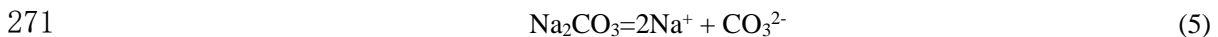
274 *2.2.4. Sulfate activators*

275   At present, neutral salt is considered by researchers to be a suitable activator because it can

276 avoid efflorescence caused by high alkalinity, short construction time and potential impact on the

277 environment. Because the pH of the sulfate solution is low, it is often used to stimulate high calcium

278 precursors (e.g. pH of Na_2SO_4 solution about 8) (Rashad et al., 2013). Although the pH value of the

279 Na_2SO_4 solution is low, the pH value of the paste obtained by mixing it with the GGBS can reach

280 12.0–12.5, which is significantly higher than the pH value of the GGBS-water solution (8.0–10.0)

281 (Rashad et al., 2013). This may be because the exchange between ions or the hydration reaction of

282 the calcium-silicate phase in the GGBS is improved. In general sulfate activation system, the

283 precipitate mainly includes ettringite, calcium sulfate, AFt and AFm (Deng et al., 2020). Since the

284 pH value of the solution of sulfate activators is low (Fernández-Jiménez et al., 2006), the reaction

285 rate of the activation system is slow, but when $Al_2(SO_4)_3$ is used as an activator, the cation Al^{3+} is

286 hydrolyzed into $Al(OH)_4^-$ (lowering the pH value), thereby improving the reaction speed of the

287   system. In addition, Hajimohammadi et al (2010). also found that the rapid dissolution of Al^{3+}

288   hindered the dissolution of Si^{2+}.

289   *2.2.5. Other activators*

290   Borate (e.g. $Na_2B_4O_7$) is also often used as an activator, and its alkalinity is relatively weak.

291   For example, the pH value of $Na_2B_4O_7 \cdot 10H_2O$ water solution (0.1–4.0%) is 9.2–9.3, therefore,

292   borate is often used in combination with hydroxide activators (e.g. NaOH) (Smith and McBroom.

293   2020). Tetraborate and NaOH generate perborate. It is generally thought that when borate and

294   NaOH are mixed, the effect of NaOH is better when the concentration is 4–8 M (Smith and

295   McBroom. 2020). The boron atom in the borate usually replaces the Al in the precursor. However,

296   some areas think that boric acid is harmful to health, so its application is limited. In addition, some

297   researchers also dissolve $Al(OH)_3$ in an alkaline activator (i.e. NaOH, KOH) to prepare alkali

298   aluminates, thereby obtaining corner-sharing AlO_4 tetrahedra with a three-dimensional network.

299   It has become a trend to use natural solid waste to replace AAs, because it is relatively eco-

300   friendly and has not been well utilized. The main components of natural alternative activators are

301   shown in Table 3. They are usually solid waste materials made of silica and alkali metal oxides,

302   which can be adopted as sustainable substitutes for commercial alkali silicates and alkali hydroxides.

303   The composition of most alternative activators has been described in Chapter 2.1. The pH value of

304   the alternative activator solution is often higher (≥ 10), and this type of activator often has a higher

305   potassium oxide content (i.e. Biomass ash). Olive biomass ash contains 17–33% K_2O, which makes

306   its solution pH above 13.0, so it can be used to replace activators such as KOH (Alonso et al., 2019).

307   Meanwhile, Al_2O_3 and SiO_2 in the olive biomass ash may participate in the reaction, and most of

308   the olive biomass ash has a porous structure with internal curing effect. De Moraes Pinheiro et al.

309   (2018) used olive biomass ash to successfully activate GGBS binder had similar or higher

310   compressive strength than NaOH/KOH-activated GGBS binder. The stalks of crops tend to have

311   higher potassium content, while leaves have lower potassium content. For biomass ash with low

312   potassium content, its pH value is often low, so it cannot be directly used to replace AAs, but it can

313   be used to partially replace activators or act as water glass (Si source). RHA is a low-potassium

314   biomass ash representative, and its aqueous solution has a pH value between 8.02 and 10.86. Bouzón

315   et al. (2014) used the reflux method to prepare a mixed solution of RHA and NaOH, and found that

316   the compressive strength of the fluid catalytic cracking catalyst residue sample activated by the

mixed activator could reach 31–41 MPa, which was similar to the reference mortar activated by the mixture with water glass and NaOH. The pH of WGP and RHA are similar (about 10), so researchers often use it to replace water glass to prepare AAMs. For low-alkaline siliceous waste (e.g. RHA, WGP), researchers often use chemical means to extract the Si element and prepare an alkaline activator. The hydrothermal method is one of the most common methods. WGP is dissolved in NaOH solution at a temperature of 25–100 °C or ground state in a ball mill, and placed for several hours to several days, and finally filtered and cooled to obtain AA (Kamseu et al., 2017). Of course, in the hydrothermal treatment process, the concentration and type of alkali, reaction temperature, type and fineness of silicon-rich powder, mixing and stirring time are important factors that determine the efficiency of silica extraction. Generally, increasing the fineness and reaction temperature of the silicon-rich powder can increase the solubility of SiO_2, but the effect of increasing the concentration of NaOH is not obvious. In addition, some researchers have also extended the method based on the hydrothermal method and proposed some new methods (thermochemical-fusion method), which is similar to the hydrothermal method, except that the solid NaOH and silicon-rich powder need to be mixed in advance (El-Naggar and El-Dessouky. 2017). In the process of bauxite mining, a large amount of Bayer liquor and red mud (RM) are also produced, both of which are relatively alkaline and have the potential to be used as an alternative activator (Ye et al., 2016). The pH of RM can reach 10.0–12.5, and it mainly contains iron, calcium, aluminum, silicon, and titanium. However, unlike other waste residues rich in alkali metals, the sodium content of RM varies greatly (0.4–20.0%), which may be affect the stability of the activator. In addition, some industrial wastes are also considered as alternative activators, for example, paper sludge, water glass sludge, and distillation waste from the Solvay process production of sodium carbonate, as presented in Table 3.

Table 3. Overview of the properties of alternative activators.

Alternative activator	SiO_2	Al_2O_3	CaO	K_2O	Fe_2O_3	SO_3	MgO	Na_2O*	LOI	pH	Ref.
RHA	85.58-90.2	0.25-0.38	0.91	1.59	0.21-0.82	0.19	0.32	0.19	6.69	8.02-10.86	Bouzón et al. (2014); Font et al. (2020); Varela Milla et al. (2013); He et al. (2017)

											References
			1.83	3.39		0.26	0.5				
WGP	68.7-77.5	1.6-2.6	7-13.8	0.6-1.0	0.1-1.9	0.5-1.7		7.5-14.3	0.2-0.6	10.2	El-Naggar and El-Dessouky. (2017); Jiang et al. (2019); Tho-In et al. (2018); Torres-Carrasco and Puertas. (2015); Lu et al. (2020)
OBA	5.2-23.6	0.7-5.5	20.6-27.8	17.3-32.1	3.5-6.1	0.8-4.0	0.7-1.3	13.4-19	13.1-13.5		Alonso et al. (2019); De Moraes Pinheiro et al. (2018); Font et al. (2020)
RM	3.9-19.7	16.4-24.0	2.4-11.2	0.0-0.7	16.3-39.3	0.7	0.3	2.6-13.4	8.7-14.3	10-12.5	Ye et al. (2016); Li et al. (2019b); Ye et al. (2016)
Bayer liquor	–	18.4-35.6	–	–	–	–	–	23.2-24.8	–	–	Jamieson et al. (2016). Jamieson et al. (2015)
Paper sludge	0.7	1	95.1	–	0.1	–	0.8	–	50	–	Mengasini et al. (2021); Adesanya et al. (2018)
Soda waste	2.4	1.2	59.5	0.1	0.7	3.3	2	4.8	51	10-12	Bilginer et al. (2020)
MSA	21	1	3	30	<1	1	4	<1	30	12-13	Peys et al., (2016)
MCA	18	1	1	32	<1	1	2	–	37	13-14	Peys et al., (2016)
CSA	8.3	1.2	5.3	32.4	0.6		23.2	0.7	7.3	11-13.3	Balo et al. (2018)
Oak/beech ash	2	<1	35	8	<1	3	4	<1	45	13	Peys et al., (2016)

*The chemical composition in the table only includes the chemical composition of the material when it is used as a substitute activator; OBA: Olive biomass ash, MSA: Maize stalk ash; MCA: Maize cob ash; CSA: Calcined cotton shell ash.

3. Performance influencing factors

3.1. Types and concentration of alkali activators

The performance of AAM mainly depends on the raw materials' fineness, composition, soluble silicon-aluminum content, etc., among which the composition and content of the glass phase are

345   very important. Generally, the glass phase in the precursor only quickly dissolves in an alkaline

346   environment and forms a gel. Therefore, the types of AAs have an important influence on the

347   composition, setting time and strength of hydration products. It is known that the hydration product

348   formed by stimulating the precursor material with sodium or potassium-based AA is mainly K-A-

349   S-H or N-A-S-H according to the mechanism of alkali-activated reaction. The hydration product

350   formed by stimulating the precursor material with calcium-based AA is mainly C-A-S-H or C-S-H

351   or the mixture of the two. In sodium or potassium-based AAs, the radius of sodium ions is smaller

352   than that of potassium ions, resulting in differences in the generated gel speed and hardening time

353   (Rahier et al., 2007). As presented in Fig. 9, for the mixed paste of GGBS, FA and RHA, the

354   activation rate of the strong base NaOH is faster, which leads to the decrease of fluidity (Karim et

355   al., 2015). Among the three activators ($Ca(OH)_2$, KOH and NaOH), the activation rate of $Ca(OH)_2$

356   is relatively slower, which means that the dissolution rate of the glass phase is slower. Scientists

357   have confirmed that the structural stability and corrosion resistance of AAMs prepared by sodium

358   hydroxide is better than potassium hydroxide. However, the mechanical properties of AAMs

359   generated by potassium-based AA are better than sodium-based. The cost of potassium-based AAs

360   is usually higher than that of sodium-based. When the sodium silicate is used as an AA, it can not

361   only provide hydroxide ions but also Si-O, can participate the formation of K-A-S-H or N-A-S-H,

362   and is conducive to the formation of three-dimensional network gel of $[SiO_4]$ (Yan et al., 2021).

363   Therefore, the single or mixture type-AA is selected according to the requirements of the project.

364   In addition, some researchers adjust the hardening rate and mechanical properties of AAM by

365   adjusting the ratio of Na_2CO_3, NaOH and Na_2SiO_3, as presented in Fig. 10 (Fernández-Jiménez et

366   al., 2003). However, Luo et al. (2014) found that the microstructure of the GGBS-FA binder

367   prepared using Na_2CO_3 and Na_2SiO_3 was not as dense as the system activated by NaOH and Na_2SiO_3.

368   Fernández-Jiménez et al. (2003) systematically studied the performance evolution of the Na_2CO_3-

369   NaOH-Na_2SiO_3 activated binder system, and found that when the Na_2CO_3 content increased, the

370   setting time of AAM was prolonged but the mechanical properties remained basically unchanged,
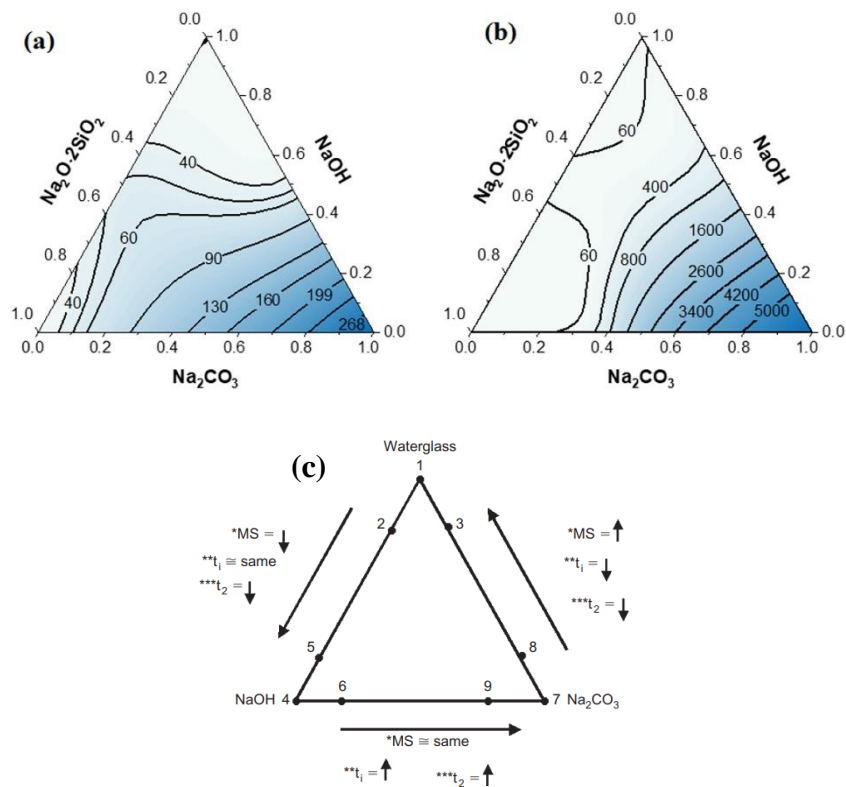
371   as presented in Fig. 10(c).
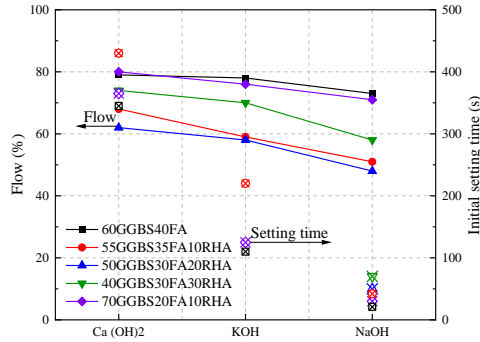
372

373 Fig. 9. The effect of activator type (2.5 M) on the fluidity and setting time of GGBS-FA-RHA paste (Karim et

374 al., 2015).

375

376

377 Fig. 10. The effect of Na₂CO₃-NaOH-Na₂SiO₃ activators on the setting time of AAM. (a) initial setting time, (b)

378 final setting time. (c) in which MS is compressive strength; t_i is initial setting time; t_2 is the time of exothermic

379 peak of the main product appears (Shi et al. 2019a; Fernández-Jiménez et al., 2003).

380   The concentration of the AA affects the dissolution rate of Al_2O_3 and SiO_2 in the precursor

381 material and the mechanical properties of the AAM. When the concentration of the AA is low, the

382 concentration of hydroxide ions produced is also low, and the ability of nucleophilically attacking

383 covalent bonds of Al-O and Si-O is weakened. It is difficult to form more Al $(OH)_4^-$ and $Si(OH)_4$.

384 Meanwhile, the concentration of metal ions is also low, which detrimental to the formation of gel

structure. The performance of the AAM formed by activating the precursor material with a low concentration of the AA decreases. Therefore, it is necessary to determine a reasonable concentration of AAs to optimize the performance of the AAM. For example, the anti-chloride ion performance, strength, and heat of hydration of AAMs increases with the increase of the concentration of AAs (Wang et al., 2005). AAMs have more compact matrix when the concentration of the AA is increased (Acevedo-Martinez et al., 2012). However, an excessively high concentration of the AA will reduce the workability and mechanical properties of the AAM. Generally, the optimal concentration of the AA is determined under specific test conditions. For example, the hydration of GGBS can be effectively activated when the pH of the mixture solution is higher than 11.5 (Song et al., 2000). For the MK component activated by NaOH, the reaction exotherm curve is shown in Fig. 11 (Zhang et al., 2012a). The first peak is the dissolution exotherm of MK in alkaline solution. The second peak is the heat released by the polymerization of aluminate and silicate monomers to form the gel. As the molar concentration of NaOH increases, the exothermic heat of the AAM component increases significantly, which means that the reaction rate of the system increases. As presented in Fig. 12, the two new bands respectively represent the asymmetric stretching vibration of the Si-O-T chain in the AAM backbone and the asymmetric stretching vibration of the non-bridging oxygen site (Zhang et al., 2012a). With the increase of NaOH concentration, the two new bands move to lower wavenumbers, which indicates that the degree of transformation of Al from the non-tetrahedral in MK to the Si-bonded tetrahedral in the AAM framework becomes higher. However, there is no uniform standard for the choice of the modulus of NaOH because of the difference in the material composition. Some researchers use lower molar concentration NaOH (3 M) to activate the FA-GGBS system, and some scholars believe that high molar concentration NaOH (10 M) has a better effect on strengthening the mechanical properties of FA-based AAM (Huiskes et al., 2016). Generally speaking, there is an optimal molar concentration of NaOH for the activation effect of AAM. As the molar concentration of sodium hydroxide increases, the performance of AAM first increases and then decreases. Aliabdo et al. (2016a) found that the AAM prepared by using 16 M NaOH had higher strengths than the AAM prepared by 12 M and 18 M NaOH. For the ratio of NaOH to Na_2SiO_2, the range of 0.4 to 4.5 is adopted by researchers, but the ratio of 2.0–2.5 is relatively more. Of course, there is also an optimal number for the ratio of NaOH to Na_2SiO_2 for alkali activation, as presented in Fig. 13.
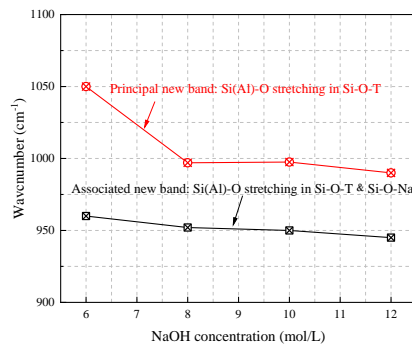
415
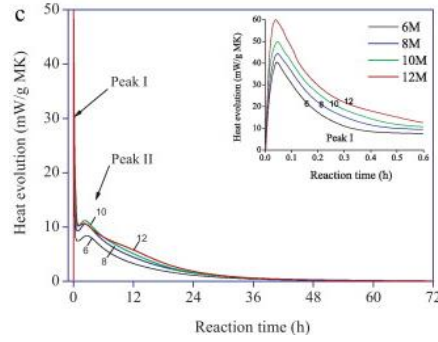
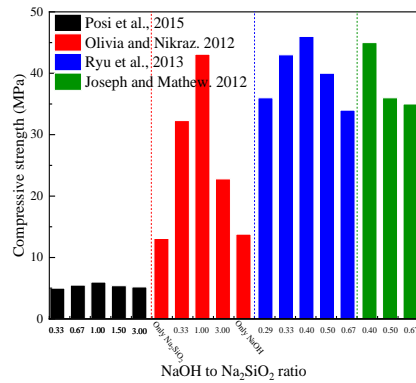Fig. 11. Effects of molar concentration of NaOH on heat evolution of MK-AAM at 30 °C (Zhang et al.,

2012a).

418

Fig. 12. The effect of NaOH concentration on the positions of the new band (resolved principal and the associated)

in the FTIR deconvolution (Zhang et al., 2012a).

421

Fig. 13. The effect of NaOH to Na_2SiO_2 on the strengths of AAM (Posi et al., 2015; Olivia and Nikraz. 2012;

Ryu et al., 2013; Joseph and Mathew. 2012).

3.2. Ratio of Si/Na/K to Al

The ratio of Si/Na/K to Al will affect the strengths and microstructure of AAMs. In the alkali-

activated reaction, the Al can promote the reaction rate, the Si can promote the growth of strength,

and Na/K contributes to the formation and stability of the three-dimensional network gel structure.

Therefore, the performance of the AAM can be improved by adjusting the ratio of Si/Na/K to Al.

429   For example, an appropriate increase in the ratio of Si/Na/K to Al can make uniform and dense for

430   gels structure, which can improve the strengths of the AAM. At the low ratio of Si and Al, the AAM

431   has a fast setting and hardening rate after the polycondensation reaction of $Al(OH)_4^-$ and $Si(OH)_4$.

432   On the contrary, its setting and hardening times are relatively long. Steveson et al. (2005) prepared

433   AAMs with a Si/Al of 4, and found that when the Si/Al ratio increased from 3 to 4, the compressive

434   strength of the samples increased from 16 to 48 MPa, and the specimens with high Si/Al ratio had

435   a denser microstructure (Fig. 14).
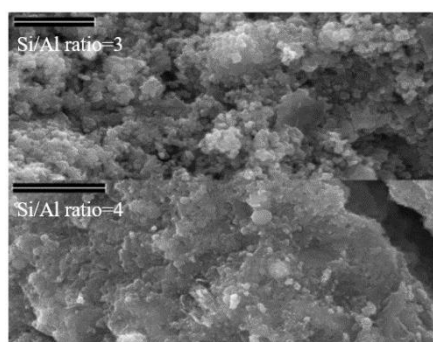
436

437   Fig. 14. The microstructure of AAM with difference Si/Al ratios (Steveson and Sagoe-Crentsil. 2005).

438   In the AAM, the $Al(OH)_4^-$ unit has a negative charge, and a positively charged Na/K ion is

439   required to combine with it electrostatically to form a complete unit system. Therefore, 1 mol of

440     $Al(OH)_4^-$ unit needs to be combined with 1 mol of Na/K ion. When the ratio of Na/K to Al is small,

441   the mechanical properties of AAMs will be reduced. When it is higher, excessive Na/K ions will

442   cause the resulting gel phase to crystallize, thereby reducing its mechanical properties. If elements

443   Si and Al in the precursor material can be completely dissolved and participate in the reaction under

444   the action of the AA, the optimal ratio of Si and Al, Na/K and Al is 2 and 1, respectively e (Zhang

445   et al., 2020). In fact, there will always be some precursor materials that do not participate in the

446   reaction in the alkali-activated reaction system, and the final mechanical properties of the AAM

447   depend on the soluble Si and Al e (Zhang et al., 2020). The highest strength of the FA-based AAM

448   are required to achieve when the ratios of SiO_2/Al_2O_3 and SiO_2/Na_2O are 2 and 5, respectively

449   (Bhagath Singh and Subramaniam, 2019). Zhang et al. (2012a) discussed the effect of Na/Al ratio

450   on the performance of AAM by isothermal calorimetry and other microstructure testing methods,

451   and found that when Na/Al ratio was less than 1.0, increasing the Na/Al ratio had a significant effect

452   on improving the reaction degree of MK system (Fig. 15). Meanwhile, Zhang et al., (2012a) also

453   found that although increasing the ratio of Na/Al ratio could increase the reaction rate of the MK
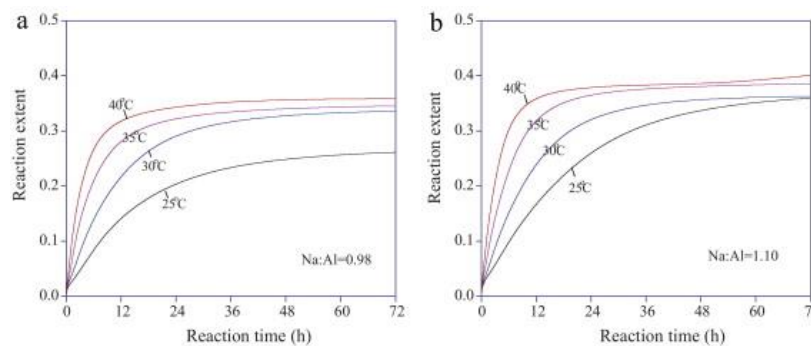
454 system at different temperatures (25–40 °C), the high Na/Al ratio made the effect of temperature on

455 its final reaction degree lower, as presented in Fig. 16.
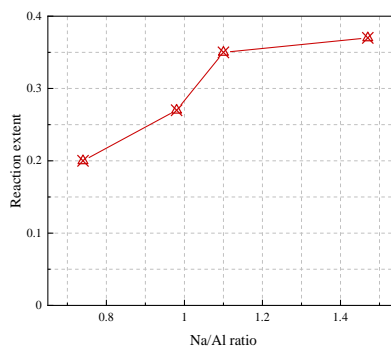
456

457   Fig. 15. The influence of Na/Al ratios on the reaction extent of MK system (Zhang et al., 2012a).

458

459   Fig. 16. The influence of Na/Al ratios and temperature on the reaction extent of MK system by isothermal

460   conduction calorimetry (Zhang et al., 2012a).

461 *3.3. Content of Ca*

462   In the calcium-based AAM, the content of Ca has different effects on the performance of the

463 AAMs. When the content of Ca is high, calcium ions enters the polycondensation chain and reduce

464 the polymerization degree of the aluminosilicate gel phase, thereby reducing the mechanical

465 properties of AAMs, and the shrinking deformation increases (Gomez-Zamorano et al., 2017). On

466 the contrary, it is detrimental to the formation of C-S-H, and it will also cause the mechanical

467 properties of AAMs to decrease. A proper content of Ca will promote the formation of C-S-H, and

468 the AAM has similar properties to cement. Therefore, it is necessary to determine the ratio of

469 calcium to silicon through experiments, so that the AAM has good properties in terms of mechanics,

470 heat resistance, crack resistance, and carbonization resistance. For example, the thermal shrinkage

471 resistance of the FA-based AAM is the best when the content of calcium hydroxide is 8% at high

472 temperature (Dombrowski et al., 2007). Dombrowski et al. also found that in the $Ca(OH)_2$-FA

473 system, with the increased of $Ca(OH)_2$ content to 8%, the mechanical properties and high

474   temperature resistance of AAM were improved, as shown in Fig. 17 (Dombrowski et al., 2007).

475   This was mainly due to the presence of aluminosilicate network phase and a small amount of

476   hydrated calcium silicate phase in AAM with $Ca(OH)_2$. Meanwhile, the $Ca(OH)_2$, as the germ of

477   the system reaction, accelerated the hydration rate of the product. In addition, Li et al. (2019) found

478   that in the SiO_2-Al_2O_3-CaO system, as the calcium content increased, the reaction rate of the GGBS-

479   AAM system increased. This study presented that in AAM, calcium was a network modifier that

480   accelerated the dissolution rate of available precursors, as presented in Fig. 18.
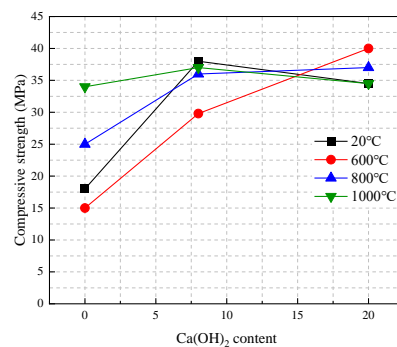
481

482   Fig. 17. Compressive strength of FA-AAM at 111d (Dombrowski et al., 2007).

483
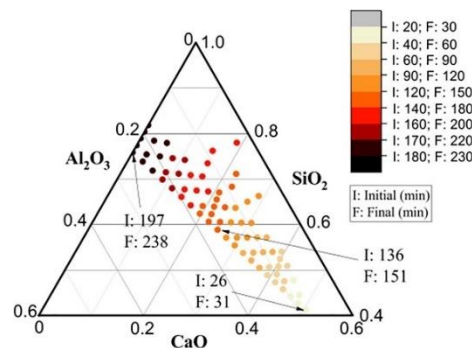
484

485   Fig. 18. Setting time of AAM in SiO_2-Al_2O_3-CaO system (Shi et al. 2019a).

486   *3.4. Curing conditions*

487   AAM is generally cured at 60–100 °C for 24–48 h, and then cured at room temperature, which

488   is more stringent than the curing regime of ordinary CBMs. Aliabdo et al. (2016b) found that as the

489   curing temperature increased, the strength of FA-AAM first increased and then decreased.

490   Meanwhile, Joseph and Mathew (2012) also found that as the curing temperature increased, the

491   strength of FA-AAM first increased and then stabilized, as presented in Fig. 19. However, for

492   different precursors and activators (reaction rates of the system), the optimal curing temperature

493   was also different. Gómez-Casero et al., (2021) used KOH and K_2SiO_3 to activate biomass bottom

ash and steel slag to prepare AAM. It was found that high temperature curing (60 ℃) could

significantly increase the early-ages (~28 d) mechanical properties of AAM, but it was detrimental

to the development of long-term strengths, and the strength of the AAM was reduced in 90 days due

to the difference in the microstructure of the gel dehydration. Meanwhile, the room temperature-

cured group (20 ℃) obtained a higher 90-day compressive strength. Hoang and Do (2020)

systematically investigated the effect of the curing regime on the dissolution rate of the active

substances in the RM-FA binder, and found that with the increased of the curing temperature (50 to

200 ℃ under atmospheric pressure), the dissolution rate of active SiO_2 and Al_2O_3 in FA and RM

increased under alkaline conditions. Although the dissolution rate of SiO_2 in RM was low in alkaline

environment, it increased significantly under autoclave curing, and, the dissolution rate of SiO_2, and

Al_2O_3 also increased with the extension of curing time, as presented in Table 4. Hoang and Do (2020)

also found that with the dissolution of SiO_2 in the RM-FA system, the compressive strength of the

specimen increased linearly. Of course, prolonging the curing time under normal pressure could

also increase the compressive strength of AAM to a certain extent (Fig. 19), but when the curing

time was too long, the gain of the strength of the specimen was not obvious.
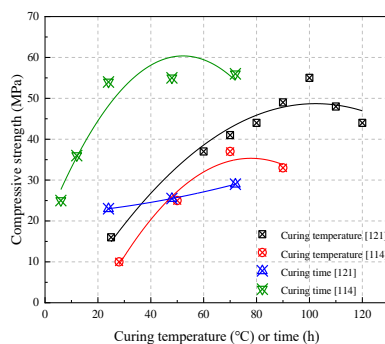
Fig. 19. The effect of the curing regimes on the compressive strength of AAM at 7 days (Joseph and Mathew.

2012; Aliabdo et al. 2016b).

Table 4. Dissolution ability of active composition after difference curing regimes.

Curing regimes			Dissolution ratio (%)			
	Temperature	Time	FA		RM	
	(℃)	(h)	Al_2O_3	SiO_2	Al_2O_3	SiO_2
	50	10	2.11	2.23	1.74	0.00
High temperature curing	100	10	3.14	3.65	2.95	0.00
	150	10	3.88	4.10	3.02	0.00
	200	10	4.25	4.37	3.22	0.00
Autoclave curing	144	10	6.25	8.34	4.25	1.28

170	10	10.25	9.69	6.25	1.87
188	10	16.35	11.65	7.98	2.38
201	10	20.25	13.72	8.45	2.89
188	4	10.33	10.33	6.42	1.95
188	8	13.65	11.46	7.02	2.08
188	12	17.98	13.00	8.33	2.44
188	16	20.33	18.25	9.03	2.98

In addition to the curing temperature and time, the researchers also investigated the performance evolution of AAM under a special curing regime (El-Feky et al., 2020). El-Hassan et al. (2021) found that for the full-volume GGBS binder, the long-term water-cured group performed better than the air-cured group and the combination of water curing and air curing group. However, for different binder systems, the optimal curing regime was also different. For 25%FA+75%GGBS binder, water cured for 2 days + subsequent air-cured group had the best performance, while for 50%FA+50%GGBS binder, water-cured group had the best performance. El-Feky et al. (2020) found that the strength of the AAM specimens cured under high temperature conditions (dry, heating in an electric oven at 80 ℃) was significantly lower than that of the water-cured group and the air-cured group. However, 2 min of microwave treatment could strengthen the compressive strength of the sample to the highest, as presented in Fig. 20. It can be seen that there are obvious differences in the optimal curing regime for different AAM systems. However, it has become a possible way to use combined curing or other new curing methods to deal with AAM.
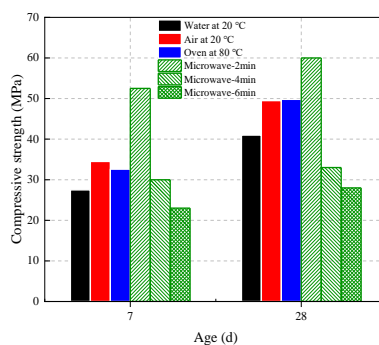
Fig. 20. The effect of curing regime on the strength of GGBS-AAM (El-Feky et al., 2020).

*3.5. Type and content of water*
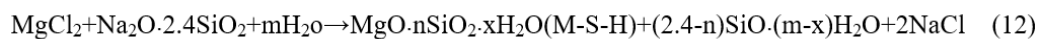
With the construction of buildings on the seashore or islands, sea sand and seawater are also used to prepare AAM, but the complex ions contained in seawater have an impact on the performance and development of AAM (Zhang et al., 2021). Water participates in the dissolution

of precursor materials and the transmission of internal ions and plays a vital role in the entire alkali-activated reaction. Seawater and tap water have different effects on the structure and strength of AAMs. This is because calcium, sodium, and potassium ions in seawater will be incorporated into the gel structure to form N-A-S-H, K-A-S-H, C-S-H and C-A-S-H or partial mixed gels, which has an important impact on the mechanical properties and durability of AAMs. Compared with tap water, seawater-based AAMs generally have well mechanical properties (Kang and Kim, 2020). However, Shi et al. (2019b) reported that although the microstructure of seawater-based AAM was not significantly different from that of tap water specimens, the strength of seawater-based AAM was significantly lower than that of tap water specimens. This is mainly due to the ion exchange between sodium silicate and seawater. As a result, soluble ions are converted into insoluble products, as presented in Fig. 21 (Shi et al., 2019b). This process is presented in Eq. (12), Cl^- and Na^+ combine to form NaCl, forming insoluble SiO_2 gel and M-S-H gel (as presented in the XRD of Fig. 21), achieving charge balance, and this process is often accompanied by a decrease in pH (from 11.30 to 11.01) and a decrease in the content of soluble silica in the solution. Therefore, the decrease of the pH value of the activator and the decrease of soluble SiO_2 hinder the strength development of AAM.
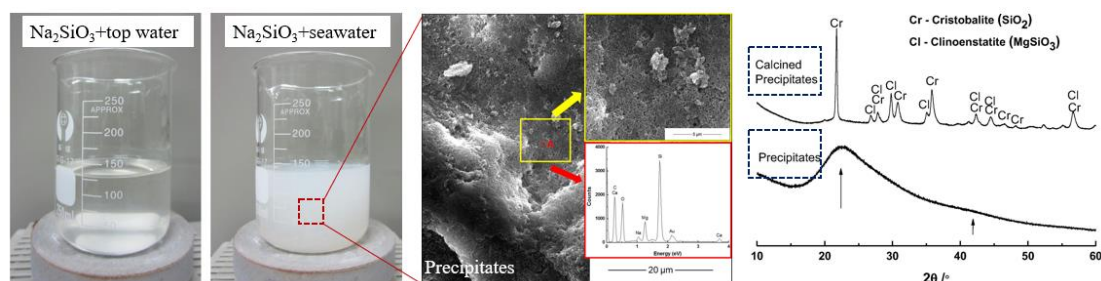
Fig. 21. The alkaline solutions composition with top water and seawater (Shi et al., 2019b).

$$MgCl_2 + Na_2O \cdot 2.4SiO_2 + mH_2o \rightarrow MgO \cdot nSiO_2 \cdot xH_2O(\text{M-S-H}) + (2.4-n)SiO \cdot (m-x)H_2O + 2NaCl \quad (12)$$

The water-binder ratio can impact on mechanical properties and durability of AAMs, as shown in Fig. 22 (Zhang et al., 2021). Whether it is seawater or ordinary water, the effect of water-binder ratio on the performance of the mixture is relatively similar. As water-binder ratio increases, the fluidity and setting time of the mixture increase. However, a small amount of liquid is detrimental to the compactness of the mixture and the dissolution of active substances of precursor, which makes its compressive strength lower. But the excess liquid increases the pore content of the hardened mixture and reduces the pH value in AAM. When the ratio of water to alkali-excited raw materials

is low, it is detrimental to the formation of AAMs, the dissolution of precursor materials, and the transmission of internal ions. Therefore, it is detrimental to strength and durability. On the contrary, excessive water makes AAMs have good fluidity and transport internal ions. However, excessive water reduces the pH of the AAM, thereby inhibiting the reaction. Meanwhile, excessive water increases internal pores and reduce strength. The best ratio of water and precursor should be determined according to the type of raw materials, particles size, workability, fluidity, viscosity, etc.
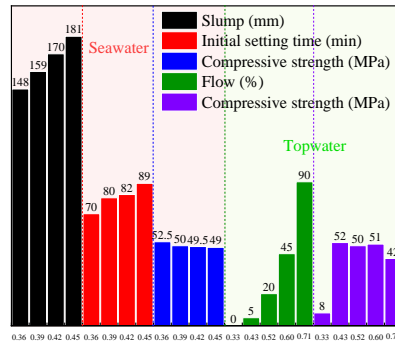

Fig. 22. The effect of water-binder ratio on the performance of AAMs (Shi et al., 2019b; Zhang et al., 2021; Sathonsaowaphak et al., 2009).

4. Sustainability evaluation

Fig. 23(a) presents carbon emissions from common precursors and activators. OPC has the highest carbon emission, which has reached 0.83 kg/kg. As a highly-reactive precursor, MK has a higher carbon footprint due to the calcination process. From the perspective of reactivity and carbon emission, FA and GGBS are still better choices. Compared to the precursor, the carbon emission of the activator is higher. Meanwhile, the most commonly used sodium silicate and sodium hydroxide have the highest carbon emissions, forcing researchers to develop more eco-friendly activators. Salt activators and alkaline solid wastes have become alternative activators. The carbon emissions of AAMs are calculated based on previous studies (Shi et al., 2021a), as shown in Fig. 23(b). Incorporating solid waste into AAM can significantly reduce its carbon footprint (Fořt et al., 2018; Shi et al., 2021a). The carbon emissions of OPC blends are still significantly higher than that of AAM. Shah et al. (2021) used lithium slag powder to prepare AAM with 39% lower carbon emissions than OPC mixture. Meanwhile, Ma et al. (2018, 2019 and 2020) developed a series of one-component activators to replace traditional activators and found that the carbon emissions of AAM were significantly reduced. Compared with commercial activators, seeking alternative activators is still an effective way to reduce the environmental burden of AAM. Mellado et al. (2014)

used sodium hydroxide reflux, RHA-based activator to prepare AAM, and found that its carbon footprint was reduced by about half compared to commercial water glass-based AAM. Gao et al. (2017) also used olivine nano-silica instead of silicate and concluded that the CO_2 emissions of the activator were reduced by 20.4–29.0% compared to commercial water glass. It can be seen that the development of sustainable activators is the key to the production of low-carbon AAMs, but there are limited studies on the life cycle assessment of novel activators-AAMs.
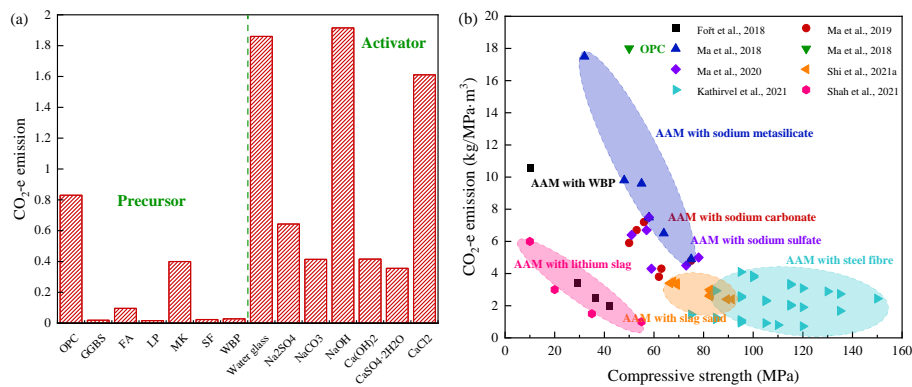
Fig. 23. Environmental assessment of raw material (a) and AAMs (b). LP: limestone powder, SF: silica fume, WBP: waste brick powder (Kathirvel et al., 2021; Ma et al., 2018, 2019 and 2020).

5. Conclusions and prospects

AAMs are a kind of low-carbon building materials. On the one hand, they can realize the disposal and resource utilization of industrial solid waste and the requirements of sustainable development. On the other hand, they have similar properties to cement, has broad application prospects in the field of civil engineering, such as sustainable construction materials, repair materials, protective coatings, low-cost ceramic materials, porous thermal insulation, functional composite materials. Researchers have done a lot of basic research on the preparation and parameter optimization of alkali-activated cementitious materials (AAMs) and achieved fruitful results. Although researchers have done a lot of work on the performance enhancement of AAMs, the shrinkage deformation, flowering, phase stability and its long-term effects still need to be further studied. The following conclusions and prospects can be drawn:

(1) AAMs are a type of low-carbon building cementitious materials. The alkali activator (AA) activates the precursor material to generate the AAM through the combined process of decomposition and polycondensation. It is unquestionable that more green and sustainable

608   precursors and AA materials will be widely used in the future, but their related reaction mechanisms

609   and derivative problems need to be further resolved.

610   (2) Different alkali/alkaline-earth metal-based AAs can activate precursor materials to generate

611   different types of cementitious materials. The type and concentration of AAs, the ratio of Si/Na/K

612   to Al, the content of Ca, and the type and content of water can have a greater impact on the

613   performance of the AAM. The ratio of Si/Na/K to Al will affect the internal structure and

614   mechanical properties of AAMs.

615   (3) The performance indicators such as strength, impermeability, and durability need to be

616   considered when AAMs are prepared. In the AAM, scientists need to systematically study and

617   determine the systemic reaction mechanism and stable performance indicators, and formulate

618   relevant theories and industry standards, so that AAMs will become common building cementing

619   materials in the field of civil engineering.

620   (4) It is beneficial to develop low-cost precursors and activators, and it is a challenge to use

621   activators with low environmental impact to prepare AAM with similar properties. The performance

622   of AAMs is often difficult to meet application requirements. Their overall performance had to be

623   improved through physical or chemical modification. For example, the crack resistance of AAMs

624   can be improved by adding fibers and admixtures. The factors affecting the performance of OPC

625   should be considered into AAMs, a systematic theory and industry standards for alkali-activated

626   mortar and concrete have been established.

627   (5) The mechanism of alkali-activated reaction is complicated, which is different from the hydration

628   reaction of cement and the polymerization reaction of organic matter. The mechanism should be

629   studied through current testing techniques, big data techniques, theoretical models, and other

630   methods. Clarifying the alkali-activated mechanism under different raw materials. By summarizing,

631   the systemic mechanism of the alkali-activated reaction is obtained.

632   (6) The performance of AAMs prepared from the same raw material fluctuates greatly due to the

633   different sources of raw materials. By accumulating preparation data, raw materials and

634   proportioning standards should be formulated, is similar with the preparation of OPC, to guide the

635   preparation of AAMs with dense structure, excellent performance and meeting engineering

636   requirements.

637

Conflict of interest

The authors state that there is no conflict of interest.

Author contribution

Xiaoniu Yu contributed to the conception of the study; Jinyan Shi and Zhihai He performed the experiment and the data; Qiang Yuan performed the data analyses and wrote the manuscript; Osman Gencel and Cong Ma helped perform the analysis with constructive discussions.

Data availability

The datasets used and/or analyzed during the current study are available from the corresponding author on reasonable request.

Declarations

Ethics approval and consent to participate Not applicable.

Consent for publication All authors read and approved the final manuscript.

Competing interests The authors declare no competing interests.

References

Abbas, R., Khereby, M. A., Ghorab, H. Y., Elkhoshkhany, N. 2020. Preparation of geopolymer concrete using Egyptian kaolin clay and the study of its environmental effects and economic cost. Clean Technologies and Environmental Policy, 22(3), 669-687.

Acevedo-Martinez E, Gomez-Zamorano L Y, Escalante-Garcia J I, 2012. Portland cement-blast furnace slag mortars activated using waterglass: Part 1: Effect of slag replacement and alkali concentration. Constr. Build. Mater. 37, 462-469.

Adesanya E, Ohenoja K, Luukkonen T, et al. 2018. One-part geopolymer cement from slag and pretreated paper sludge. J. Clean. Prod., 185, 168-175.

Akturk B, Akca A H, Ahmet B. Kizilkanat A B, 2020. Fracture response of fiber-reinforced sodium carbonate activated slag mortars. Constr. Build. Mater. 241, 118128.

670 Albidah A S. 2021. Effect of partial replacement of geopolymer binder materials on the fresh and mechanical
671   properties: A review. Ceram. Int.

672 Alonso M M, Gascó C, Morales M M, et al. 2019. Olive biomass ash as an alternative activator in geopolymer
673   formation: A study of strength, radiology and leaching behaviour. Cement Concr. Compos., 104, 103384.

674 Aliabdo A A, Abd Elmoaty M, Salem H A. 2016a. Effect of water addition, plasticizer and alkaline solution
675   constitution on fly ash based geopolymer concrete performance. Construct. Build. Mater., 121, 694-703.

676 Aliabdo A A, Abd Elmoaty M, Salem H A. 2016b. Effect of cement addition, solution resting time and curing
677   characteristics on fly ash based geopolymer concrete performance. Construct. Build. Mater., 123, 581-593.

678 Balo A M, Rahier H, Mobili A, et al. 2018. Metakaolin-based inorganic polymer synthesis using cotton shell ash as
679   sole alkaline activator. Construct. Build. Mater., 191, 1011-1022.

680 Bouzón N, Payá J, Borrachero M V, et al. 2014. Refluxed rice husk ash/NaOH suspension for preparing alkali
681   activated binders. Mater. Lett., 115, 72-74.

682 Bhagath Singh G V P, Subramaniam K, 2019. Effect of active components on strength development in alkali-
683   activated low calcium fly ash cements. J. Sustain. Cem. Based Mater. 8, 1-19.

684 Bie R, Song X, Liu Q, et al. 2015. Studies on effects of burning conditions and rice husk ash (RHA) blending amount
685   on the mechanical behavior of cement. Cement Concr. Compos., 55, 162-168.

686 Bilginer A, Canbek O, Turhan Erdoğan S. 2020. Activation of blast furnace slag with soda production waste. J.
687   Mater. Civ. Eng., 32(1), 04019316.

688 Clausi M, Fernández-Jiménez A M, Palomo A, et al. 2018. Reuse of waste sandstone sludge via alkali activation in
689   matrices of fly ash and metakaolin. Construct. Build. Mater., 172, 212-223.

690 Cordeiro G C, Vieira A P, Lopes É S. 2017. Study on the pozzolanic activity of sugar cane straw ash produced using
691   different pretreatments. Química Nova, 40, 264-269.

692 Deng X, Guo H, Tan H, et al. 2021. Effect of organic alkali on hydration of GGBS-FA blended cementitious material
693   activated by sodium carbonate. Ceram. Int.

694 Deng G, He Y, Lu L, et al. 2020. The effect of activators on the dissolution characteristics and occurrence state of
695   aluminum of alkali-activated metakaolin. Construct. Build. Mater., 235, 117451.

696 De Moraes Pinheiro S M, Font A, Soriano L, et al. 2018. Olive-stone biomass ash (OBA): An alternative alkaline
697   source for the blast furnace slag activation. Construct. Build. Mater., 178, 327-338.

698 Dombrowski K, Buchwald A, Weil M, 2007. The influence of calcium content on the structure and thermal
699   performance of fly ash based geopolymers. J. Mater. Sci. 42, 3033-3043.

700 El-Hassan H, Shehab E, Al-Sallamin A. 2021. Effect of curing regime on the performance and microstructure
701   characteristics of alkali-activated slag-fly ash blended concrete. J. Sustain. Cem-Based Mater., 1-29.

702 El-Feky M S, Kohail M, El-Tair A M, et al. 2020. Effect of microwave curing as compared with conventional
703   regimes on the performance of alkali activated slag pastes. Construct. Build. Mater., 233, 117268.

704 Fernández-Jiménez A, Palomo A, Sobrados I, et al. 2006. The role played by the reactive alumina content in the
705   alkaline activation of fly ashes. Microporous Mesoporous Mater., 91(1-3), 111-119.

706 Fernández-Jiménez A, Puertas F. 2003. Effect of activator mix on the hydration and strength behaviour of alkali-
707   activated slag cements. Adv. Cem. Res., 15(3), 129-136.

708 Font A, Soriano L, de Moraes Pinheiro S M, et al. 2020. Design and properties of 100% waste-based ternary alkali-
709   activated mortars: Blast furnace slag, olive-stone biomass ash and rice husk ash. J. Clean. Prod., 243, 118568.

710 Fu Q, Xu W, Zhao X, et al. 2021. The microstructure and durability of fly ash-based geopolymer concrete: A review.
711   Ceram. Int.

712 Fořt, J., Vejmelková, E., Koňáková, D., Alblová, N., Čáchová, M., Keppert, M., Černý, R. (2018). Application of
713   waste brick powder in alkali activated aluminosilicates: Functional and environmental aspects. Journal of
714   cleaner production, 194, 714-725.

715 Garcia-Lodeiro I, Palomo A, Fernández-Jiménez A. 2015. An overview of the chemistry of alkali-activated cement-
716   based binders. Handbook of alkali-activated cements, mortars and concretes, 19-47.

717 Gbozee M, Zheng K, He F, et al. 2018. The influence of aluminum from metakaolin on chemical binding of chloride
718   ions in hydrated cement pastes. Appl. Clay Sci., 158, 186-194.

719 Geng Y, Wang Z, Shen L, et al., 2019. Calculating of CO_2 emission factors for Chinese cement production based
720   on inorganic carbon and organic carbon, J. Clean. Prod. 217, 503-509.

721 Gomez-Zamorano L, Balonis M, Erdemli B, et al., 2017. C-(N)-S-H and N-A-S-H gels: Compositions and solubility
722   data at 25°C and 50°C. J. Am. Ceram. Soc. 100, 2700-2711.

723 Gómez-Casero M A, Pérez-Villarejo L, Castro E, et al. 2021. Effect of steel slag and curing temperature on the
724   improvement in technological properties of biomass bottom ash based alkali-activated materials. Construct.
725   Build. Mater., 302, 124205.

726 Gao, X., Yu, Q. L., Lazaro, A., Brouwers, H. J. H. (2017). Investigation on a green olivine nano-silica source based
727   activator in alkali activated slag-fly ash blends: reaction kinetics, gel structure and carbon footprint. Cement
728   and Concrete Research, 100, 129-139.

729 Gavali, H. R., Bras, A., Ralegaonkar, R. V. 2021. Cleaner construction of social housing infrastructure with load-
730   bearing alkali-activated masonry. Clean Technologies and Environmental Policy, 23(8), 2303-2318.

731 Hajimohammadi A, Provis J L, Van Deventer J S J. 2010. Effect of alumina release rate on the mechanism of
732   geopolymer gel formation. Chem. Mater., 22(18), 5199-5208.

733 Hanjitsuwan S, Hunpratub S, Thongbai P, et al. 2014. Effects of NaOH concentrations on physical and electrical
734   properties of high calcium fly ash geopolymer paste. Cement Concr. Compos., 45, 9-14.

735 He Z, Li L, Du S. 2017. Creep analysis of concrete containing rice husk ash. Cement Concr. Compos., 80, 190-199.

736 Hoang M D, Do Q M. 2020. Effect of curing regime on properties of red mud based alkali activated materials.
737   Construct. Build. Mater., 259, 119779.

738 Huiskes D M A, Keulen A, Yu Q L, et al. 2016. Design and performance evaluation of ultra-lightweight geopolymer
739   concrete. Mater. Design, 89, 516-526.

740 Jamieson E, Kealley C S, Van Riessen A, et al. 2016. Optimising ambient setting Bayer derived fly ash geopolymers.
741   Materials, 9(5), 392.

742 Jamieson E, McLellan B, Van Riessen A, et al. 2015. Comparison of embodied energies of Ordinary Portland
743   Cement with Bayer-derived geopolymer products. J. Clean. Prod., 99, 112-118.

744 Joseph B, Mathew G. 2012. Influence of aggregate content on the behavior of fly ash based geopolymer concrete.
745   Sci. Iran., 19(5), 1188-1194.

746 Kang S H, Hong S G, Moon J. 2019. The use of rice husk ash as reactive filler in ultra-high performance concrete.
747   Cement Concr. Res., 115, 389-400.

748 Kamseu E, à Moungam L M B, Cannio M, et al. 2017. Substitution of sodium silicate with rice husk ash-NaOH
749   solution in metakaolin based geopolymer cement concerning reduction in global warming. J. Clean. Prod., 142,
750   3050-3060.

751 Karim M R, Zain M F M, Jamil M, et al. 2015. Development of a zero-cement binder using slag, fly ash, and rice
752   husk ash with chemical activator. Adv. Mater. Sci. Eng., 2015.

753 Kang C, Kim T, 2020. Pore and strength characteristics of alkali-activated slag paste with seawater. Mag. Concrete
754   Res. 72, 499-508.

Kogbara R.B., Al-Tabbaa A., 2011. Mechanical and leaching behaviour of slag-cement and lime-activated slag stabilised/solidified contaminated soil. Sci. Total Environ. 409, 2325-2335.

Kathirvel, P., Sreekumaran, S. (2021). Sustainable development of ultra high performance concrete using geopolymer technology. Journal of Building Engineering, 39, 102267.

Lang L, Chen B, Chen B. 2021. Strength evolutions of varying water content-dredged sludge stabilized with alkali-activated ground granulated blast-furnace slag. Construct. Build. Mater., 275, 122111.

Lertwattanaruk P, Sua-iam G, Makul N. 2018. Effects of calcium carbonate powder on the fresh and hardened properties of self-consolidating concrete incorporating untreated rice husk ash. J. Clean. Prod., 172, 3265-3278.

Li N, Shi C, Zhang Z, et al. 2019a. A review on mixture design methods for geopolymer concrete. Compos. Part B-Eng., 178, 107490.

Li Y, Min X, Ke Y, et al. 2019b. Preparation of red mud-based geopolymer materials from MSWI fly ash and red mud by mechanical activation. Waste Manage., 83, 202-208.

Li, J., Wang, Q. 2022. Evaluation of the compressive strength and Cl$^-$ content of the blast furnace slag-soda sludge-based cementitious material using machine-learning approaches. Clean Technologies and Environmental Policy, 24(3), 983-1000.

Lu C, Zhang Z, Shi C, et al. 2021. Rheology of alkali-activated materials: A review. Cement Concr. Compos., 104061.

Luo X, Xu J, Li W, et al. 2014. Effect of alkali-activator types on the dynamic compressive deformation behavior of geopolymer concrete. Mater. Lett., 124, 310-312.

Martirena F, Monzó J. 2018. Vegetable ashes as supplementary cementitious materials. Cement Concr. Res., 11457-64.

Mañosa J, Cerezo-Piñas M, Maldonado-Alameda A, et al. 2021. Water treatment sludge as precursor in non-dehydroxylated kaolin-based alkali-activated cements. Appl. Clay Sci., 204, 106032.

Mengasini L, Mavroulidou M, Gunn M, 2021. Alkali-activated concrete mixes with ground granulated blast furnace slag and paper sludge ash in seawater environments. Sustain. Chem. Pharm. 20, 100380.

Muthadhi A, Kothandaraman S. 2010. Optimum production conditions for reactive rice husk ash. Mater. Struct., 43(9), 1303-1315.

Mellado, A., Catalán, C., Bouzón, N., Borrachero, M. V., Monzó, J. M., Payá, J. (2014). Carbon footprint of geopolymeric mortar: study of the contribution of the alkaline activating solution and assessment of an alternative route. RSC advances, 4(45), 23846-23852.

Ma, C., Zhao, B., Guo, S., Long, G., Xie, Y. (2019). Properties and characterization of green one-part geopolymer activated by composite activators. Journal of Cleaner Production, 220, 188-199.

Ma, C., Long, G., Shi, Y., Xie, Y. (2018). Preparation of cleaner one-part geopolymer by investigating different types of commercial sodium metasilicate in China. Journal of Cleaner Production, 201, 636-647.

Ma, C., Zhao, B., Wang, L., Long, G., Xie, Y. (2020). Clean and low-alkalinity one-part geopolymeric cement: effects of sodium sulfate on microstructure and properties. Journal of Cleaner Production, 252, 119279.

Nimwinya E, Arjharn W, Horpibulsuk S, et al. 2016. A sustainable calcined water treatment sludge and rice husk ash geopolymer. J. Clean. Prod., 119, 128-134.

Olivia M, Nikraz H. 2012. Properties of fly ash geopolymer concrete designed by Taguchi method. Mater. Design (1980-2015), 36, 191-198.

Peys A, Rahier H, Pontikes Y. 2016. Potassium-rich biomass ashes as activators in metakaolin-based inorganic polymers. Appl. Clay Sci., 119, 401-409.

Pham P N, Duan W, Zhuge Y, et al. 2021. Properties of mortar incorporating untreated and treated drinking water treatment sludge. Construct. Build. Mater., 280, 122558.

799 Posi P, Ridtirud C, Ekvong C, et al. 2015. Properties of lightweight high calcium fly ash geopolymer concretes
800   containing recycled packaging foam. Construct. Build. Mater., 94, 408-413.

801 Parathi, S., Nagarajan, P., Pallikkara, S. A. 2021. Ecofriendly geopolymer concrete: a comprehensive review. Clean
802   Technologies and Environmental Policy, 23(6), 1701-1713.

803 Rattanasak U, Pankhet K, Chindaprasirt P. 2011. Effect of chemical admixtures on properties of high-calcium fly
804   ash geopolymer. Int. J. Miner. Metall. Mater., 18(3), 364-369.

805 Rashad A M, Bai Y, Basheer P A M, et al. 2013. Hydration and properties of sodium sulfate activated slag. Cement
806   Concr. Compos., 37, 20-29.

807 Rahier H, Wastiels J, Biesemans M, et al. 2007. Reaction mechanism, kinetics and high temperature transformations
808   of geopolymers. J. Mater. Sci. 42, 2982-2996.

809 Ryu G S, Lee Y B, Koh K T, et al. 2013. The mechanical properties of fly ash-based geopolymer concrete with
810   alkaline activators. Construct. Build. Mater., 47, 409-418.

811 Sarde B, Patil Y D, Dholakiya B Z. 2021. Evaluation of effectiveness of palm oil fuel ash as green filler and methyl
812   methacrylate as additive in recycled PET resin polymer composite. J. Build. Eng., 43, 103107.

813 Saleh A A, Abdel-Gawwad H A, Abd EL-Moghny M G, et al. 2021. The sustainable utilization of weathered cement
814   kiln dust in the cleaner production of alkali activated binder incorporating glass sludge. Construct. Build. Mater.,
815   300, 124308.

816 Sathonsaowaphak A, Chindaprasirt P, Pimraksa K. 2009. Workability and strength of lignite bottom ash geopolymer
817   mortar. J. Hazard Mater., 168(1), 44-50.

818 Shi J, Tan J, Liu B, et al. 2021. Experimental study on full-volume slag alkali-activated mortars: Air-cooled blast
819   furnace slag versus machine-made sand as fine aggregates. J. Hazard Mater., 403, 123983.

820 Shi C, Qu B, Provis J L. 2019a. Recent progress in low-carbon binders. Cement Concr. Res., 122, 227-250.

821 Shi J, Liu B, Liu Y, et al. 2020. Preparation and characterization of lightweight aggregate foamed geopolymer
822   concretes aerated using hydrogen peroxide. Construct. Build. Mater., 256, 119442.

823 Smith R A, McBroom R B. 2000. Boron oxides, boric acid, and borates. Kirk-Othmer Encyclopedia of Chemical
824   Technology,

825 Song S, Sohn D, Jennings H M, et al. 2000. Hydration of alkali-activated ground granulated blast furnace slag. J.
826   Mater. Sci. 35, 249-257.

827 Steveson, M., Sagoe-Crentsil, K., 2005. Relationships between composition, structure and strength of inorganic
828   polymers. J. Mater. Sci. 40, 4247-4259.

829 Sun X, Guo S, Dai Q, et al. 2017. Microstructure characterization of alkali-glass particle and alkali-glass powder
830   reacted gels with neutron scattering and imaging techniques. Mater. Charact., 131, 98-107.

831 Shi D, Yao Y, Ye J, et al. 2019b. Effects of seawater on mechanical properties, mineralogy and microstructure of
832   calcium silicate slag-based alkali-activated materials. Construct. Build. Mater., 212569-577.

833 Shah, S. F. A., Chen, B., Ahmad, M. R., Haque, M. A. (2021). Development of Cleaner One-part geopolymer from
834   lithium slag. Journal of Cleaner Production, 291, 125241.

835 Tahri W, Hu X, Shi C, et al. 2021. Review on corrosion of steel reinforcement in alkali-activated concretes in
836   chloride-containing environments. Construct. Build. Mater., 293, 123484.

837 Temuujin J, Minjigmaa A, Davaabal B, et al. 2014. Utilization of radioactive high-calcium Mongolian flyash for the
838   preparation of alkali-activated geopolymers for safe use as construction materials. Ceram. Int., 40(10), 16475-
839   16483.

840 Tho-In T, Sata V, Boonserm K, et al. 2018. Compressive strength and microstructure analysis of geopolymer paste
841   using waste glass powder and fly ash. J. Clean. Prod., 172, 2892-2898.

842 Torres-Carrasco M, Puertas F. 2015. Waste glass in the geopolymer preparation. Mechanical and microstructural
843   characterisation. J. Clean. Prod., 90, 397-408.

844 Varela Milla O, Rivera E B, Huang W J, et al. 2013. Agronomic properties and characterization of rice husk and
845   wood biochars and their effect on the growth of water spinach in a field test. J. Soil Sci. Plant Nut., 13(2), 251-
846   266.

847 Venkatanarayanan H K, Rangaraju P R. 2015. Effect of grinding of low-carbon rice husk ash on the microstructure
848   and performance properties of blended cement concrete. Cement Concr. Compos., 55, 348-363.

849 Wang A, Zheng Y, Zhang Z, et al. 2020. The durability of alkali-activated materials in comparison with ordinary
850   portland cements and concretes: a review, Engineering, 6(6), 695-706.

851 Wang H, Li H, Yan F, 2005. Synthesis and mechanical properties of metakaolinite-based geopolymer. Coloid.
852   Surface. A. 268, 1-6.

853 Wianglor K, Sinthupinyo S, Piyaworapaiboon M, et al. 2017. Effect of alkali-activated metakaolin cement on
854   compressive strength of mortars. Appl. Clay Sci., 141, 272-279.

855 Xue L, Zhang Z, Wang H, 2021. Hydration mechanisms and durability of hybrid alkaline cements (HACs): A review.
856   Constr. Build. Mater. 266, 121039.

857 Yan Z, Sun Z, Yang J, et al. 2021. Mechanical performance and reaction mechanism of copper slag activated with
858   sodium silicate or sodium hydroxide, Constr. Build. Mater. 266, 120900.

859 Ye N, Chen Y, Yang J, et al. 2016. Co-disposal of MSWI fly ash and Bayer red mud using an one-part geopolymeric
860   system. J. Hazard Mater., 318, 70-78.

861 Yu X, Wang Z, Wang J. 2022, Mechanical properties of bio-cementation materials in pre-precipitation mixing
862   process. Environ Sci Pollut Res, 29(1): 1314-1323.

863 Yu X, Jiang J. Mineralization and cementing properties of bio-carbonate cement, bio-phosphate cement, and bio-
864   carbonate/phosphate cement: a review. Environ Sci Pollut Res, 2018, 25(22): 21483-21497.

865 Zhang D, Wang A, 2020. Review on property of geopolymer binder and its engineering application. J. Archit. Civ.
866   Eng., 37, 13-38.

867 Zhang J, Shi C, Zhang Z, et al. 2017. Durability of alkali-activated materials in aggressive environments: A review
868   on recent studies. Construct. Build. Mater., 152, 598-613.

869 Zhang Z, Wang H, Provis J L, et al. 2012a Quantitative kinetic and structural analysis of geopolymers. Part 1. The
870   activation of metakaolin with sodium hydroxide. Thermochim. Acta, 539, 23-33.

871 Zhang B, Zhu H, Shah K W, et al. 2021. Optimization of mix proportion of alkali-activated slag mortars prepared
872   with seawater and coral sand. Construct. Build. Mater., 284, 122805.

873 Zhang Z, Yao X, Wang H. 2012b Potential application of geopolymers as protection coatings for marine concrete
874   III. Field experiment. Appl. Clay Sci., 67, 57-60.